Journal of Power Sources 202 (2012) 394–399

Contents lists available at SciVerse ScienceDirect

Journal of Power Sources

journal homepage: www.elsevier.com/locate/jpowsour

Short communication

Synthesis and electrochemical properties of a sulfur-multi walled carbon nanotubes composite as a cathode material for lithium sulfur batteries

Wook Ahn [a], Kwang-Bum Kim [a], Kyu-Nam Jung [b], Kyoung-Hee Shin [b], Chang-Soo Jin [b,*]

[a] Department of Materials Science & Engineering, Yonsei University, 50 Yonsei-ro, Seodaemun-Gu, Seoul 120-749, Republic of Korea
[b] Korea Institute of Energy Research, 152 Gajeong-ro, Yuseong-Gu, Daejeon 305-343, Republic of Korea

ARTICLE INFO

Article history:
Received 4 October 2011
Received in revised form
18 November 2011
Accepted 20 November 2011
Available online 6 December 2011

Keywords:
Sulfur
CNTs
Lithium sulfur
Battery
Cathode

ABSTRACT

A sulfur-multi walled carbon nanotubes (MWCNTs) composite is prepared by the direct precipitation method as a cathode material for lithium sulfur batteries. The microstructure and morphology of the sulfur-MWCNTs composite are characterized by means of X-ray diffraction (XRD), scanning electron microscopy (SEM), energy dispersive X-ray spectrometer (EDS) mapping and thermogravimetric analysis (TGA). From these results, it is found that the synthesized sulfur has an orthorhombic phase and the MWCNTs are chemically well-dispersed over the whole surface of the synthesized sulfur. Electrochemical charge–discharge tests demonstrated that the sulfur-MWCNTs composite exhibits better capacity retention (63%) than that (16%) of the precipitated sulfur, which is also prepared by the direct precipitation method without MWCNTs. The enhanced cycle performance of the sulfur-MWCNTs is mainly attributed to the formation of highly conductive electron path due to the uniformly dispersed MWCNTs. Furthermore, in order to investigate the electrochemical reaction mechanism for the Li–S cell during the discharge process, the ac-impedance spectra as a function of the state of discharge are measured and analyzed.

1. Introduction

Lithium rechargeable batteries require increasingly high power and energy density due to the development of high performance portable electric devices, electric vehicles, and battery energy storage systems. In relation to this, lithium sulfur batteries have attracted much interest due to their high theoretical specific capacity of 1672 mAh g^{-1} and theoretical energy density of 2600 Wh kg^{-1} based on cathode materials [1,2]. Furthermore, on the basis of advantages such as low cost, abundance in nature, and environment friendliness, sulfur is one of the most promising cathode candidates for lithium rechargeable batteries with high energy density [3].

However, in spite of these advantages, prior to the commercialization of lithium sulfur batteries, there are numerous problems that must be overcome. It is generally known [4] that the electrical insulating nature of sulfur, the soluble polysulfide reaction in the organic based electrolyte, and low utilization of sulfur are responsible for the rapid capacity decay of lithium sulfur batteries [5–11]. Therefore, enhancing the cycling performance and improving sulfur utilization are important factors with respect to the realization of high energy lithium sulfur batteries. It has been argued that the key to solving these critical problems is to prepare a rigid composite of sulfur and a conducting material by uniformly incorporating sulfur into a conducting matrix [12–14].

Recently, many attempts to incorporate sulfur into an electrical conducting carbon matrix have been made in efforts to enhance the cycle performance of lithium sulfur batteries. Notably, it was reported [15,16] that chemical dispersion of conducting carbon materials such as acetylene black and carbon nanotubes (CNTs) with sulfur reinforces the electric conductivity of the cathode and effectively prevents the dissolution of lithium polysulfide into the electrolyte, This indicates that the utilization of sulfur as a cathode material is improved during the charge–discharge process. In the present work, a well-dispersed sulfur-multi walled carbon nanotubes (MWCNTs) composite was simply synthesized via direct precipitation route in order to enhance the electrical conduction properties of sulfur, the microstructure and surface morphology of that composite were characterized and the effects of the dispersed-MWCNTs on the electrochemical performance of the sulfur-MWCNTs composite were then investigated. In addition, from an analysis of the ac-impedance spectra measured on the sulfur-MWCNTs composite, the electrochemical reaction behavior of the lithium sulfur cell during the discharge process was also examined.

2. Experimental

2.1. Sulfur-MWCNTs composite synthesis

To prepare a sulfur-MWCNTs composite by the direct precipitation method [17], first, acid treated MWCNTs (HANOS CM-95,

* Corresponding author. Tel.: +82 42 860 3271; fax: +82 42 860 3133.
E-mail address: csjin@kier.re.kr (C.-S. Jin).

0378-7753/$ – see front matter © 2011 Elsevier B.V. All rights reserved.
doi:10.1016/j.jpowsour.2011.11.074

Hanwha Nanotech Co.) were dispersed in a 0.1 M $Na_2S_2O_3$ (sodium thiosulfate) solution. The purchased MWCNTs are synthesized by using thermal CVD method and its specific surface area is about 500–1000$m^2\,g^{-1}$. To effectively disperse the MWCNTs with $Na_2S_2O_3$, sonication was carried out for 2 h. Then, 0.1 M H_2SO_4 was added dropwise at a rate of 10 ml min^{-1} to the solution, which was stirred for 1 h. The reaction formula for the sulfur preparation is as follows:

$$Na_2S_2O_3 + H_2SO_4 \rightarrow Na_2SO_4 + S\downarrow + H_2SO_3 \quad (1)$$

After filtration, the precipitated sulfur-MWCNTs compound was washed by distilled water repeatedly and the resulting composite was finally obtained by evaporation of the solvent and drying at 60 °C for 2 h. To attain sulfur content of 80 wt% in the resulting sulfur-MWCNTs composite, the amount of MWCNTs was appropriately adjusted. A reference sulfur sample without MWCNTs was also synthesized by the same precipitation method.

2.2. Material characterization

For characterizing the weight ratio of the sulfur-MWCNTs composite, a thermogravimetric analysis (TGA/SDTA851^e-METTLER) was performed on the composite in a temperature range of 40–600 °C with a heating rate of 5 °C min^{-1} under a nitrogen gas atmosphere. In order to identify the crystal structure of the sulfur-MWCNTs composite powder, X-ray diffraction (XRD) patterns were recorded with an automated HPC-2500 XRD diffractometer (Gogaku) using Cu K_α radiation (λ = 1.5405 Å). The measurements were conducted over a scanning angle 2θ range of 10–80° using a step width of 0.02° at a scanning rate of 2° min^{-1}. To determine the surface morphology, scanning electron microscopy (SEM) was performed with a cold field emission SEM S4700 (Hitachi).

2.3. Cell assembly and characterization of sulfur-MWCNTs composite

To prepare a cathode electrode for electrochemical testing, a composite powder of sulfur-MWCNTs and acetylene black was mixed with PVdF-co-HFP (Kynar 2801) in N-methyl pyrrolidinone (NMP) solution. The composite electrode consisted of 70 wt% sulfur-MWCNTs, 10 wt% conducting material and 20 wt% binder. This slurry was then coated on an Al foil (20 μm) and finally dried under vacuum at 60 °C for 48 h. The electrode was subsequently pressed with a twin roller and the final thickness of the coated sulfur-MWCNTs composite cathode was approximately 30 μm. In the present work, the composite electrode with MWCNTs and the reference electrode without MWCNTs are denoted as the sulfur-MWCNTs and precipitated sulfur, respectively.

Electrochemical experiments were performed in 1.0 M $LiCF_3SO_3$ and 0.2 M $LiNO_3$ in a mixture of tetra(ethylene glycol) dimethyl ether (TEGDME)/1,3-dioxolane (DOL) (50:50 vol.%) using a coin-type cell (CR2032) with a Li counter electrode. It should be noted that $LiNO_3$ was used as additive in the electrolyte to enhance the cyclability of the Li–S cell [18,19]. All the procedures for the coin cell assembly were carried out in an argon filled glove box.

The charge–discharge test was carried out with a Maccor series 4000 at a current density of 100 mA g^{-1} with a voltage range of 1.6 – 2.8 V_{Li/Li^+}. All the specific capacity values in the present work were calculated on the basis of sulfur mass. Electrochemical impedance spectra were recorded by using a Zahner IM6 with application of an ac-amplitude of 5 mV_{rms} on an open circuit potential over a frequency range from 10^5 Hz down to 10^{-2} Hz. All electrochemical experiments were carried out at room temperature.

3. Results and discussion

Fig. 1 presents the XRD patterns measured from the sulfur-MWCNTs composite and the as-received MWCNTs powder. All peak positions of the sulfur-MWCNTs composite correspond to the standard Bragg positions of the orthorhombic phase with the space group *Fddd* (JCPDS 83-2283: S_8), as shown at the bottom of Fig. 1, and no traces of other impurities were found within the detection limit of the instrument. This indicates that there are no other side reactions except for sulfur precipitation during the composite preparation. In addition, it was also found that the base line of XRD peaks around *ca.* 26° is slightly raised. This is ascribed to the dispersed MWCNTs, and indicates that a homogenous mixture of sulfur-MWCNTs was synthesized by the direct precipitation method.

In order to quantify the amount of MWCNTs in the sulfur-MWCNTs composite, a TGA analysis was carried out. Fig. 2 shows the TGA results of the sulfur-MWCNTs composite powder from 40 to 600 °C under a nitrogen atmosphere. There are two weight loss stages in the TGA curve for that composite sample. The first stage of abrupt weight loss in a *ca.* 180–310 °C temperature range reflects sulfur decomposition, and the corresponding weight loss is approximately up to 75 wt%. The previous study on the TGA analysis of the sulfur-conducting material composite suggested that the weight

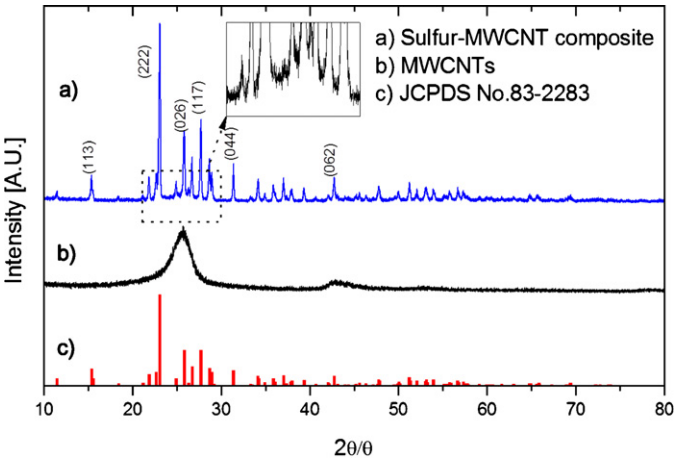

Fig. 1. XRD patterns: (a) sulfur-MWCNT composite, (b) MWCNTs and (c) JCPDS 83-2283: sulfur.

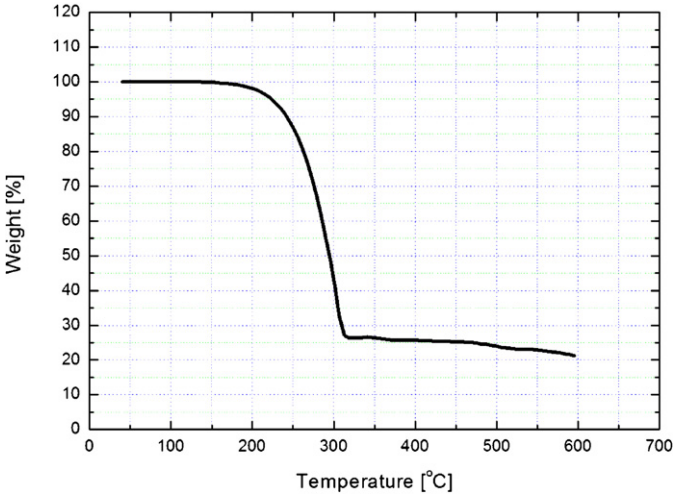

Fig. 2. TGA curve of the sulfur-MWCNT composite prepared by direct precipitation method.

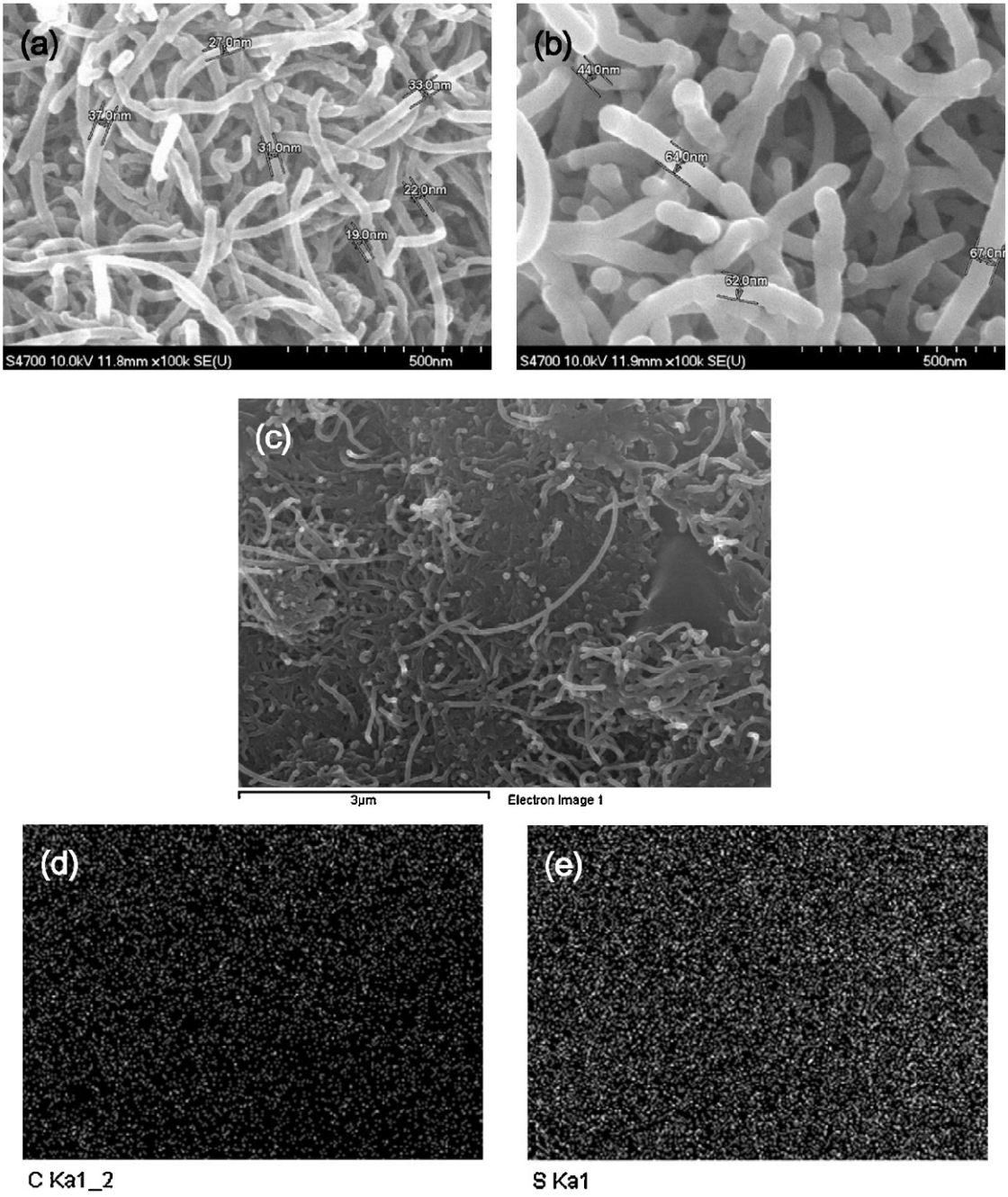

Fig. 3. SEM micrographs of (a) as-received MWCNTs and (b and c) sulfur-MWCNT composite. (d and e) Elemental mapping of sulfur-MWCNTs composite with EDS.

reduction in a *ca.* 160–280 °C temperature range is mainly due to the evaporation of the sulfur [16]. The continuative and steady weight loss of the second stage above 310 °C is estimated to be 5 wt%. Recalling that the sulfur content of the sulfur-MWCNTs composite was adjusted to 80 wt% during the preparation process and there are no impurity peaks from XRD results, it seems reasonable to attribute the weight loss of the composite sample in the second stage to the decomposition reaction of the residual sulfur.

Fig. 3(a) and (b) presents SEM micrographs of the surface morphology of the as-received MWCNTs and sulfur-MWCNTs, respectively. It should be noted that the tube diameter of the sulfur-MWCNTs composite is considerably larger than that of as-received MWCNTs, implying that the precipitated sulfur is deposited on the surface of the CNTs and formed in the hollow space of the CNTs during the sulfur-MWCNTs synthesis process. In order to verify the uniformity of MWCNTs in the composite powder, an EDS mapping analysis was used. The bright spots in Fig. 3(d) and (e) indicate the presence of the elements C and S, respectively. That EDS results demonstrate that the conductive MWCNTs are uniformly well-distributed throughout the entire surface of the sulfur-MWCNTs composite powder. Additionally, the SEM image of Fig. 3(c) also indicates that the MWCNTs are uniformly dispersed on the surface of the precipitated sulfur particles.

Fig. 4(a) displays the discharge profiles determined from the Li–S cells of the sulfur-MWCNTs composite and precipitated sulfur. All discharge curves in Fig. 4(a) exhibit two potential plateaus near 2.45 and 2.05 V (vs. Li/Li^+). The appearance of these plateaus in the discharge curve of the Li–S cell strongly indicates the formation of polysulfide during the discharge process. It has been reported [20–23] that the upper plateau is caused by the transformation

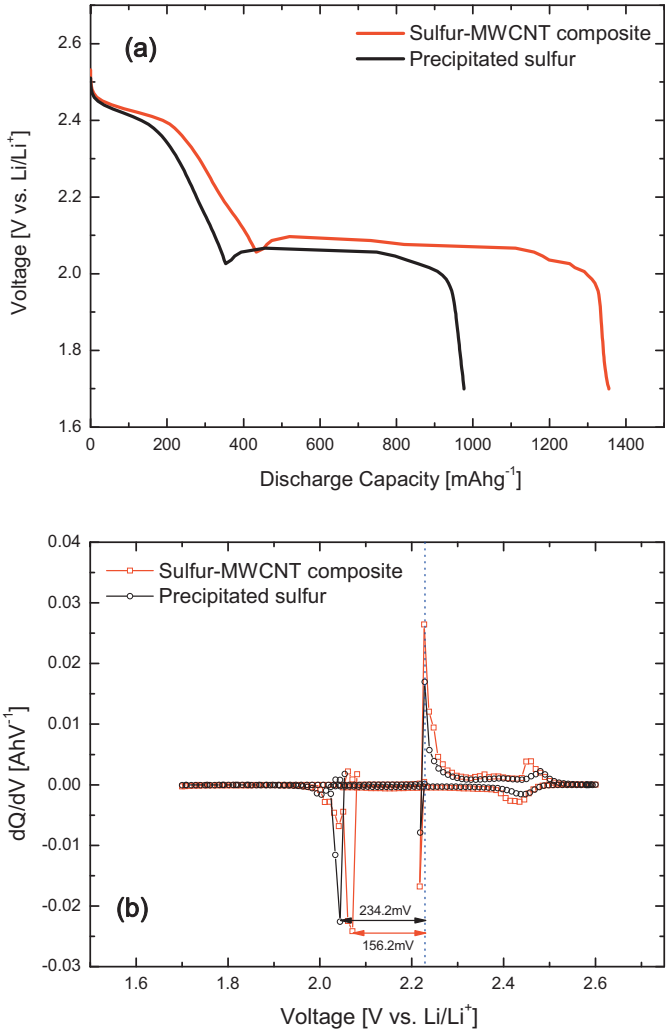

Fig. 4. (a) Discharge profiles measured with a current density of 100 mA g^{-1} for sulfur-MWCNT composite and precipitated sulfur and (b) plot of dQ/dV vs. V reproduced from the 1st charge–discharge curves.

from elemental sulfur to high-order lithium polysulfide (Li_2S_n, $4 \le n \le 8$), which is soluble in the electrolyte, and the lower plateau is ascribed to the formation of insoluble low-order lithium polysulfide (Li_2S_n, $n < 4$). The discharge reaction formula for the sulfur is as follows:

$$\text{Upperplateaureaction}: nS + 2Li^+ + 2e^- \rightarrow Li_2S_{(n-1)} + S(4 \le n \le 8) \quad (2)$$

$$\text{Lowerplateaureaction}: Li_2S_n + 2(n-1)Li^+ + 2(n-1)e^- \rightarrow nLi_2S(n < 4) \quad (3)$$

Plots of differential capacity (dQ/dV) vs. potential (V) reproduced from the 1st discharge–charge profiles obtained from the sulfur-MWCNTs composite and precipitated sulfur are presented in Fig. 4(b). Two pairs of peaks are observed on the dQ/dV vs. V plot at around 2.45 and 2.1 V (vs. Li/Li$^+$) during charge and discharge. These peaks correspond to the two potential plateaus depicted in Fig. 4(a), and are characteristic of the formation of high-order (Li_2S_n, $4 \le n \le 8$), and low-order (Li_2S_n, $n < 4$) lithium polysulfides, respectively. In Fig. 4(b), ΔV_p denotes the difference between the peak potentials of the lower plateau reaction, and represents the sum of polarizations upon charge and discharge.

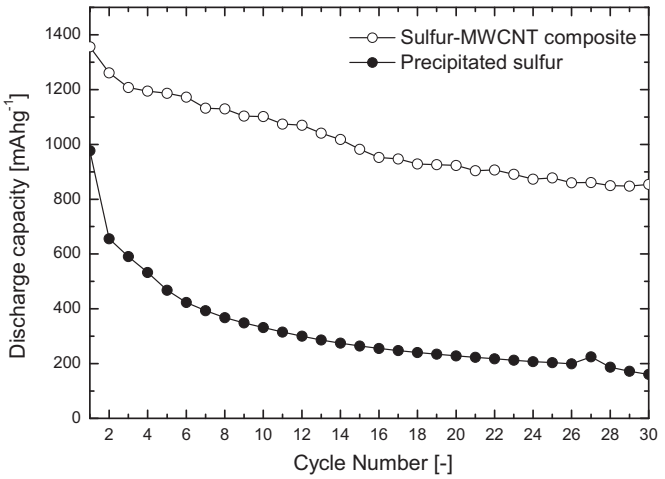

Fig. 5. Plots of discharge capacities vs. cycle number measured for the sulfur-MWCNT composite and precipitated sulfur electrodes.

In addition, the cycle performances of the Li–S cells with the sulfur-MWCNTs composite and precipitated sulfur are presented in Fig. 5. In the case of the precipitated sulfur, it is clearly seen that the discharge capacity decays drastically upon cycling. The sulfur-based Li–S cell exhibits an initial capacity of 976 mAh g^{-1} and the discharge capacity declines significantly to 160 mAh g^{-1} after 30 cycles. On the contrary, the specific discharge capacity of the Li–S cell with the sulfur-MWCNTs decreases monotonously from 1355 mAh g^{-1} to 854 mAh g^{-1} after 30 cycles.

The following three points should be noted in relation to Figs. 4 and 5: first, the 1st discharge capacity of sulfur-MWCNTs was measured to be 1355 mAh g^{-1}, which is much larger than the value (976 mAh g^{-1}) of the precipitated sulfur. If the theoretical capacity of sulfur is assumed to be 1672 mAh g^{-1}, then the sulfur utilization of sulfur-MWCNTs is 81%. Second, the value of ΔV_p determined from the sulfur-MWCNTs is 156 mV which is much smaller than the value (234 mV) measured from the precipitated sulfur. This indicates that the precipitated sulfur was subjected to substantially higher polarization during charge–discharge as compared with the sulfur-MWCNTs composite. Lastly, the capacity retention of the sulfur-MWCNTs after 30 cycles was measured to be 63%, which is much larger than the value (16%) of the precipitated sulfur; this indicates that the Li–S cell with sulfur-MWCNTs provides excellent cycle performance. Bearing in mind that the sulfur is uniformly coated on the MWCNTs and the conducting material is well dispersed over the entire composite electrode, as shown in Fig. 3, it is reasonable to attribute the high sulfur utilization, low polarization, and enhanced capacity retention of the sulfur-MWCNTs composite to the facile kinetics of the charge-transfer reaction due to highly conductive electron paths, which originate from the well-dispersed MWCNTs.

In order to comprehensively investigate the reaction mechanism of the Li–S cell with the sulfur-MWCNTs composite, the ac-impedance spectra were measured as a function of the state of discharge. Fig. 6(a) and (b) illustrate typical Nyquist plots of the ac-impedance spectra obtained from the Li–S cell with sulfur-MWCNTs at various depths of discharge (DoD), as indicated in Fig. 6(c), during the 1st discharge cycle. It was found that the measured ac-impedance spectra consist of two separated arcs in the high and intermediate frequency ranges and a straight line inclined at a constant angle to the real axis (Warburg impedance) in the low frequency range.

It has been reported [24] that the first arc is mainly caused by the formation of a surface film on the lithium and sulfur electrode, originating from the interactions between the electrode and

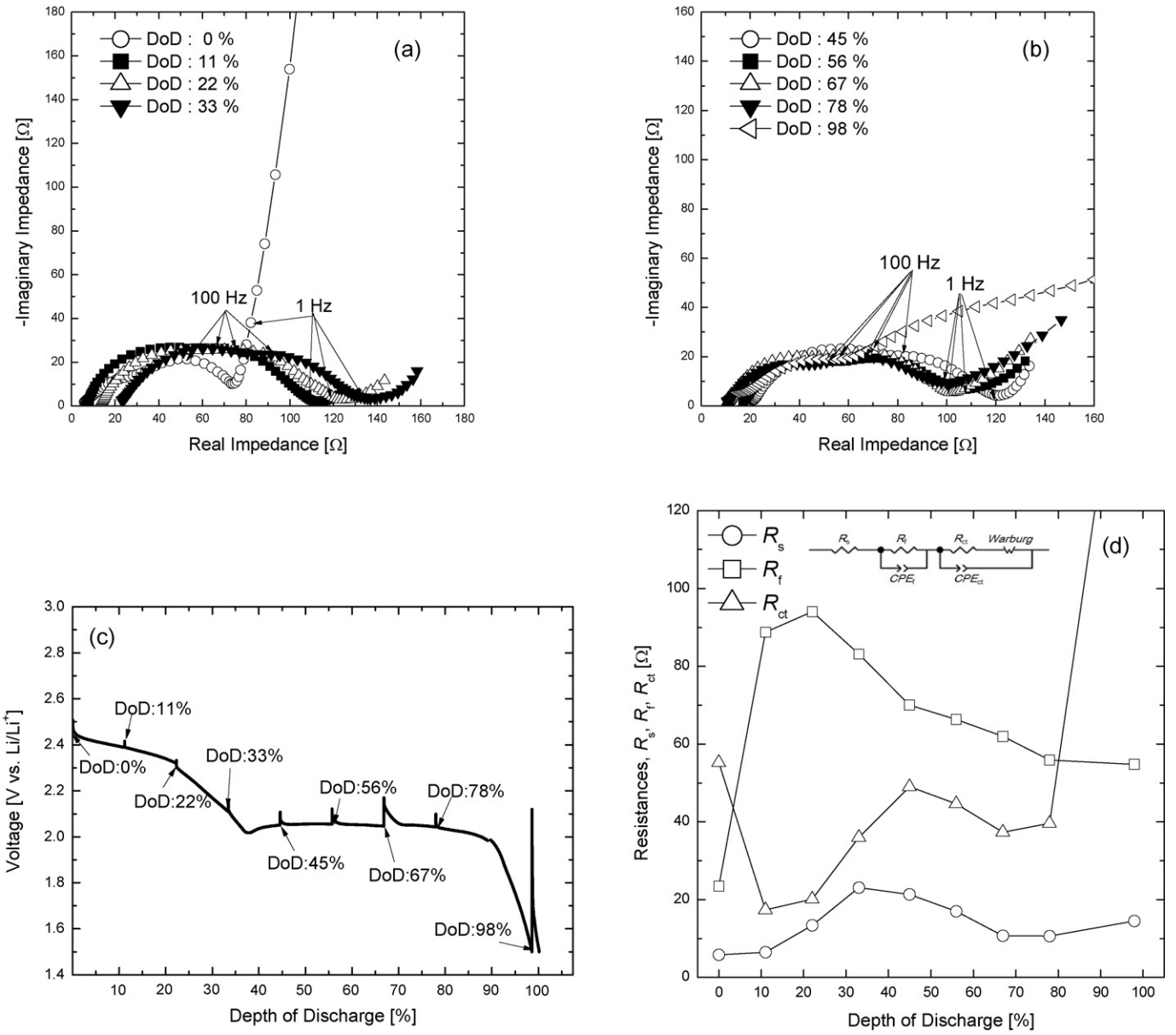

Fig. 6. (a and b) Nyquist plots of the ac-impedance spectra measured on the sulfur-MWCNT composite as a function of the depth of discharge, (c) the discharge-profiles during 1st discharge cycle and (d) plots of the electrolyte solution resistance R_s, the surface film resistance R_f and the charge-transfer resistance R_{ct} against the depth of discharge.

electrolyte solvent. The formation of a resistive film on the electrode surface in a non-aqueous organic solution is reported to be a common phenomenon [25,26]. The second arc in the intermediate frequency is ascribed to the charge-transfer reaction at the interface between the surface film and the sulfur electrode. In addition, the Warburg impedance is associated with semi-infinite diffusion of soluble lithium polysulfide in the electrolyte.

In order to quantitatively analyze the ac-impedance spectra, the electrolyte solution resistance (R_s), the surface film resistance (R_f), and charge-transfer resistance (R_{ct}) were determined at various depths of discharge according to the equivalent circuit, as given in Fig. 6(d). It should be noted that all the values of resistive components such as R_s, R_f and R_{ct} vary with the state of discharge. In particular, the electrolyte solution resistance, R_s, increases in value to 33% of DoD, which corresponds to the end point of the upper plateau reaction on the discharge curve of Fig. 6(c), and then decreases over the entire state of discharge. As the upper plateau reaction proceeds, the sulfur transforms to soluble high-order lithium polysulfide, and thus the concentration of the dissolved lithium polysulfide in the electrolyte increases. The increased concentration of the dissolved lithium polysulfide in the electrolyte strongly affects the viscosity of the electrolyte, resulting in a decrease of the electrolyte conductivity [27]. On the other hand, the subsequent decrease of the electrolyte solution resistance is ascribed to a decreased concentration of the dissolved high-order lithium polysulfide resulting from its reduction to insoluble low-order lithium polysulfide during the lower plateau reaction.

In addition, it is seen that the variations of R_f and R_{ct} determined with the state of discharge, which show the local maximum at around 22 and 45% of DoD, respectively, are in good agreement in form with the variation of R_s. In a previous study [28], the impedance behavior for the lithium sulfur battery was extensively studied during the charge and discharge process; the dependence of the resistive components on the state of discharge reported in

that study corresponds well with that of the present work. It was reported that the surface film resistance is strongly related with the ionic conduction process through the surface film on the electrode, which mainly consists of the non-conductive porous lithium sulfide. Thus, the ionic conductivity of the surface film is strongly affected by the migration of the lithium ions in the electrolyte solution as these ions occupy the pores of the surface film. Moreover, it has been well documented [27–31] that the charge-transfer reaction may significantly depend on the surface properties of the electrode and also may be strongly affected by the surface film covering the electrode surface. Consequently, it was recognized that the local maximum point of R_f and R_{ct}, at which the concentration of the dissolved lithium polysulfide in the electrolyte is high, can be attributed to the kinetic impediments of the lithium ion migration and the interfacial charge-transfer reaction in the presence of the resistive surface film, which impregnates the electrolyte with high viscosity. This implies that the discharge process of the Li–S cell is significantly influenced by the formation reaction of lithium polysulfide in the electrolyte.

4. Conclusion

A homogeneous and well dispersed sulfur-MWCNTs composite for lithium sulfur batteries was synthesized by a simple direct precipitation method and the electrochemical properties of the composite were studied. From XRD and SEM results, it was confirmed that the synthesized sulfur, which is deposited on the surface and/or formed in the hollow space of MWCNTs, has an orthorhombic phase. The sulfur-MWCNTs composite exhibits excellent performance with high specific capacity up to 1355 mAh g^{-1} at the initial discharge capacity and improved cycle durability. The improvement in the electrochemical performance is attributed to facile kinetics of the charge-transfer reaction that likely originated from the formation of highly conductive electron paths. Additionally, from the analysis of the ac-impedance spectra obtained with the state of discharge, it was suggested that the dissolved lithium polysulfide in the electrolyte plays a crucial role in the overall variation of resistance of the lithium sulfur cell. Based on the enhanced cycle performance, it was concluded that the sulfur-MWCNTs composite synthesized by a direct precipitation route is a promising cathode material for rechargeable lithium sulfur batteries.

Acknowledgement

This work was supported by the Next Generation Military Battery Research Center program of The Defense Acquisition Program Administration and Agency for Defense Development.

References

[1] D.Marmorstein, T.H. Yu, K.A. Streibel, F.R. Mclarnon, J. Hou, E.J. Cairns, J. Power Sources 89 (2000) 219–226.
[2] M.Y. Chu, U.S. Patent 5,814,420 (1998).
[3] J.O. Besenhard, Handbook of Battery Materials, Wiley-VCH, 1998.
[4] R.D. Rauh, K.M. Abraham, G.F. Pearson, J.K. Surprenant, S.B. Brummer, J. Electrochem. Soc. 126 (1979) 523–527.
[5] H. Yamin, E. Peled, J. Power Sources 9 (1983) 281–287.
[6] B. Jin, J.U. Kim, H.B. Gu, J. Power Sources 117 (2003) 148–152.
[7] A. Hayashi, T. Ohtomo, F. Mizuno, K. Tadanaga, M. Tatsumisago, Electrochem. Commun. 5 (2003) 701–705.
[8] J.H. Shin, K.W. Kim, H.J. Ahn, J.H. Ahn, Mater. Sci. Eng. B 95 (2002) 148–156.
[9] H. Yamin, J. Penciner, A. Gorenshtain, M. Flam, E. Peled, J. Power Sources 14 (1985) 129–134.
[10] T. Skotheim, U.S. Patent 5,601,947 (1997).
[11] V. Merritt, T. Sawyer, Inorg. Chem. 9 (1970) 211–215.
[12] X. Ji, K.T. Lee, L.F. Nazar, Nat. Mater. 8 (2009) 500–506.
[13] C. Liang, N.J. Dudney, J.Y. Howe, Chem. Mater. 21 (2009) 4724–4730.
[14] X. Yu, J. Xie, J. Yang, H. Huang, K. Wang, Z. Wen, J. Electroanal. Chem. 573 (2004) 121–128.
[15] J.J. Chen, X. Jia, Q.J. She, C. Wang, Q. Zhang, M.S. Zheng, Q.F Dong, Electrochim. Acta 55 (2010) 8062–8066.
[16] C. Wang, J.J. Chen, Y.N. Shi, M.S.Zheng, Q.F. Dong, Electrochim. Acta 55 (2010) 7010–7015.
[17] R.G. Chaudhuri, S. Paria, J. Colloids Interface Sci. 343 (2010) 439–446.
[18] Y.V. Mikhaylik, U.S. Patent 7,354,689 (2008).
[19] Y.V. Mikhaylik, U.S. Patent 7,553,590 (2009).
[20] R. Okuyama, E. Nomura, J. Power Sources 77 (1999) 164.
[21] J. Broadhead, T. Skotheim, J. Power Sources 65 (1997) 213.
[22] T. Skotheim, U.S. Patent US05601947 (1997).
[23] Y.J. Choi, Y.D. Chung, C.Y. Baek, K.W. Kim, H.J. Ahn, J.H. Ahn, J. Power Sources 184 (2008) 548.
[24] E. Peled, J. Electrochem. Soc. 126 (1979) 2047.
[25] E. Peled, D. Golodnitsky, G. Ardel, J. Electrochem. Soc. 144 (1997) L208.
[26] E. Peled, D. Golodnitsky, C. Menachem, D. BarTow, J. Electrochem. Soc. 145 (1998) 3483.
[27] H.S. Ryu, H.J. Ahn, K.W. Kim, J.H. Ahn, K.K. Cho, T.H. Nam, J.U. Kim, G.B. Cho, J. Power Sources 163 (2006) 201–206.
[28] V.S. Kolosnitsyn, E.V. Kuzmina, E.V. Karaseva, S.E. Mochalov, J. Power Sources 196 (2011) 1478–1482.
[29] Y.J. Choi, Y.D. Chung, C.Y. Baek, K.W. Kim, H.J. Ahn, J.H. Ahn, J. Power Sources 184 (2008) 548–552.
[30] Y. Li, H. Zhan, S. Liu, K. Huang, Y. Zhou, J. Power Sources 195 (2010) 2945–2949.
[31] S.R. Narayanan, D.H. Shen, S. Surampudi, A.I. Attia, G. Halpert, J. Electrochem. Soc. 140 (1993) 1854–1862.